

# Structural insights into the bactericidal mechanism of human peptidoglycan recognition proteins

Sangwoo Cho\*, Qian Wang\*, Chittoor P. Swaminathan\*, Dusan Hesek†, Mijoon Lee†, Geert-Jan Boons‡, Shahriar Mobashery<sup>†§</sup>, and Roy A. Mariuzza<sup>\*§</sup>

\*Center for Advanced Research in Biotechnology, W. M. Keck Laboratory for Structural Biology, University of Maryland Biotechnology Institute, 9600 Gudelsky Drive, Rockville, MD 20850; †Department of Chemistry and Biochemistry, University of Notre Dame, Notre Dame, IN 46556; and ‡Complex Carbohydrate Research Center, University of Georgia, Athens, GA 30602

Edited by David R. Davies, National Institutes of Health, Bethesda, MD, and approved April 11, 2007 (received for review February 16, 2007)

Peptidoglycan recognition proteins (PGRPs) are highly conserved pattern-recognition molecules of the innate immune system that bind bacterial peptidoglycans (PGNs), which are polymers of alternating *N*-acetylglucosamine (NAG) and *N*-acetylmuramic acid (NAM) cross-linked by short peptide stems. Human PGRPs are bactericidal against pathogenic and nonpathogenic Gram-positive bacteria, but not normal flora bacteria. Like certain glycopeptide antibiotics (e.g., vancomycin), PGRPs kill bacteria by directly interacting with their cell wall PGN, thereby interfering with PGN maturation. To better understand the bactericidal mechanism of PGRPs, we determined the crystal structure of the C-terminal PGN-binding domain of human PGRP-I $\beta$  in complex with NAG-NAM-L-Ala- $\gamma$ -D-Glu-L-Lys-D-Ala-D-Ala, a synthetic glycopeptide comprising a complete PGN repeat. This structure, in conjunction with the previously reported NMR structure of a dimeric PGN fragment, permitted identification of major conformational differences between free and PGRP-bound PGN with respect to the relative orientation of saccharide and peptide moieties. These differences provided structural insights into the bactericidal mechanism of human PGRPs. On the basis of molecular modeling, we propose that these proteins disrupt cell wall maturation not only by sterically encumbering access of biosynthetic enzymes to the nascent PGN chains, but also by locking PGN into a conformation that prevents formation of cross-links between peptide stems in the growing cell wall.

bacteria | cell wall | crystal structure | innate immunity

The innate immune system is a host defense mechanism, evolutionarily conserved from insects to mammals, which mediates early recognition and control of invading microorganisms (1, 2). It recognizes microbes by means of pattern recognition molecules, such as Toll-like receptors and collectins, which bind unique products of microbial metabolism not produced by the host (pathogen-associated molecular patterns). Examples include lipopolysaccharide, mannans, nonmethylated CpG sequences, and peptidoglycan (PGN) (1, 2).

Peptidoglycan recognition proteins (PGRPs) are pattern-recognition molecules that bind and, in certain cases, hydrolyze PGNs of bacterial cell walls (3, 4). PGRPs are found in both invertebrates and vertebrates, but have developed different functions in different animals. Insect PGRPs are involved in the Toll receptor and Imd-signaling pathways that induce expression of antimicrobial peptides (2, 5, 6). By contrast, mammalian PGRPs do not act through host signaling pathways but are directly bactericidal (5–10). Human PGRP-I $\alpha$  and -I $\beta$  are secreted proteins with strong bactericidal activity against pathogenic and nonpathogenic Gram-positive bacteria, but not normal flora bacteria (10). They are selectively expressed in tissues exposed to the environment, including the oral cavity, intestinal tract, and skin (5). Human PGRP-S, found in polymorphonuclear leukocyte granules, is directly bactericidal for both Gram-positive and -negative bacteria (7, 8, 10). Whereas PGRP-I $\alpha$  and -I $\beta$  each comprise two tandem PGN-binding domains, PGRP-S consists of a single such domain (5, 6).

Mammalian PGRPs kill 99% of bacteria at 0.1- to 1- $\mu$ M concentrations and are therefore more potent, on a molar basis, than most antimicrobial peptides (10).

Unlike mammalian antimicrobial peptides such as defensins (11, 12), which permeabilize bacterial membranes, human PGRPs kill bacteria by interacting with their cell walls, where they are believed to interfere with PGN biosynthesis (10). In this respect, PGRPs function like glycopeptide antibiotics, including vancomycin and teicoplanin, which inhibit PGN synthesis by binding PGN or its precursors (13, 14). As cross-linked PGN provides the mechanical support necessary to prevent bacterial cells from rupturing as osmotic pressure fluctuates, interfering with cross-linking provides an effective means for disrupting the structural integrity of bacteria (13, 14).

PGNs are polymers of alternating *N*-acetylglucosamine (NAG) and *N*-acetylmuramic acid (NAM) in  $\beta$  (1–4) linkage, cross-linked by short peptide stems composed of alternating L- and D-amino acids (Fig. 1A) (3, 4). Transglycosylases catalyze polymerization of lipid II to generate the polymeric PGN unit, which is cross-linked to an existing PGN unit in the cell wall by transpeptidases (13, 14). Whereas the carbohydrate backbone is conserved in all bacteria, the peptide displays diversity. According to the residue at position 3 of the stems, PGNs are divided into two categories: L-lysine type (Lys-type) and diaminopimelate type (Dap-type). Dap-type PGN stems are usually directly cross-linked, whereas Lys-type PGN stems are interconnected by a peptide bridge that varies in length and composition in different bacteria (Fig. 1A).

Vancomycin and related glycopeptide antibiotics form a noncovalent complex with the D-Ala-D-Ala portion of cell wall PGN, resulting in steric inhibition of the transglycosylation and/or transpeptidation steps of PGN synthesis (13, 14). Although human PGRPs appear to act through a similar mechanism (10), x-ray crystallographic studies have shown that these proteins bind both the glycan and peptide portions of PGNs (6, 15), as exemplified by the structure of the C-terminal PGN-binding domain of human PGRP-I $\alpha$  (PGRP-I $\alpha$ C) bound to a muramyl pentapeptide (MPP),

Author contributions: S.C., C.P.S., S.M., and R.A.M. designed research; S.C., Q.W., and C.P.S. performed research; D.H., M.L., G.-J.B., and S.M. contributed new reagents/analytic tools; S.C., C.P.S., S.M., and R.A.M. analyzed data; and S.C., S.M., and R.A.M. wrote the paper.

The authors declare no conflict of interest.

This article is a PNAS Direct Submission.

Abbreviations: Dap-type, diaminopimelate type; GMPP, glucosamyl muramyl pentapeptide; ITC, isothermal titration calorimetry; Lys-type, L-lysine type; MPP, muramyl pentapeptide; NAG, *N*-acetylglucosamine; NAM, *N*-acetylmuramic acid; PGN, peptidoglycan; PGRP, PGN recognition protein; PGRP-I $\alpha$ C, C-terminal PGN-binding domain of human PGRP-I $\alpha$ ; PGRP-I $\beta$ C, C-terminal PGN-binding domain of human PGRP-I $\beta$ .

Data deposition: Atomic coordinates and structure factors have been deposited in the Protein Data Bank, www.pdb.org [PDB ID codes 2EAV (for PGRP-I $\beta$ C) and 2EAX (for PGRP-I $\beta$ C-GMPP)].

<sup>§</sup>To whom correspondence may be addressed. E-mail: mobashery@nd.edu or mariuzza@carb.nist.gov.

This article contains supporting information online at [www.pnas.org/cgi/content/full/0701453104/DC1](http://www.pnas.org/cgi/content/full/0701453104/DC1).

© 2007 by The National Academy of Sciences of the USA

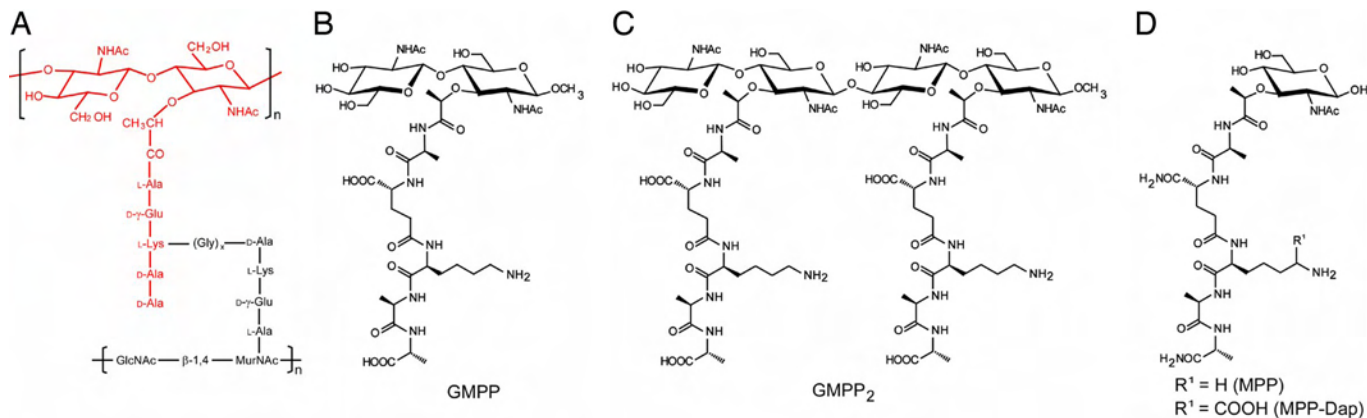


**Fig. 1.** Structure of PGN and PGN derivatives. (A) Schematic representation of Lys-type PGNs. Lys-type PGN peptides are usually cross-linked through a peptide bridge composed of one to five glycines. The fragment shown in red corresponds to GMPP. (B) Chemical structure of GMPP. (C) GMPP<sub>2</sub>. (D) MPP (R<sup>1</sup>, H) and MPP-Dap (R<sup>1</sup>, COOH).

NAM-L-Ala-γ-D-Gln-L-Lys-D-Ala-D-Ala (16). However, because MPP lacks the NAG moiety present in all PGNs, the PGRP-IαC-MPP complex only partially defined the interaction with the carbohydrate backbone of PGN. To better understand how mammalian PGRPs recognize native PGN, we determined the crystal structure of the C-terminal PGN-binding domain of human PGRP-Iβ (PGRP-IβC) in complex with NAG-NAM-L-Ala-γ-D-Glu-L-Lys-D-Ala-D-Ala, a glucosamyl MPP (GMPP) containing a complete disaccharide repeat (Fig. 1B). This structure, combined with the recent NMR structure of a dimeric PGN fragment (Fig. 1C), NAG-NAM(-L-Ala-γ-D-Glu-L-Lys-D-Ala-D-Ala)-NAG-NAM(-L-Ala-γ-D-Glu-L-Lys-D-Ala-D-Ala) (GMPP<sub>2</sub>) (17), enabled us to identify conformational changes in PGN induced by PGRP binding. These interactions suggest a mechanism whereby PGRPs disrupt cell wall maturation in a manner that is related to, yet distinct from, the mechanism used by glycopeptide antibiotics.

## Results and Discussion

**PGN Analog Binding to Human PGRPs.** The PGN-binding properties of human PGRP-IβC, as well as those of PGRP-IαC and -S, were characterized by isothermal titration calorimetry (ITC) using Lys-type PGN analogs GMPP, GMPP<sub>2</sub>, and MPP and the Dap-type analog NAM-L-Ala-γ-D-Gln-Dap-D-Ala-D-Ala (MPP-Dap) (Fig. 1B–D). ITC revealed exothermic heats of reaction for the binding of PGRP-IβC to GMPP and GMPP<sub>2</sub> [supporting information (SI) Fig. 5], with equilibrium binding constants (*K*<sub>b</sub>s) of  $2.3 \times 10^5 \text{ M}^{-1}$  and  $2.4 \times 10^5 \text{ M}^{-1}$ , respectively (Table 1). A stoichiometry of unity was observed for both reactions, indicating that GMPP<sub>2</sub>, despite being dimeric, could only accommodate a single PGRP. Significantly, vancomycin binds GMPP and GMPP<sub>2</sub> with affinities very similar to those of PGRP-IβC for these same ligands, although GMPP<sub>2</sub> engages two vancomycins (18). PGRP-IβC and -IαC have similar PGN-binding characteristics, except that PGRP-IαC recognized GMPP and GMPP<sub>2</sub> with  $\approx 4$ -fold lower *K*<sub>b</sub> than PGRP-IβC. PGRP-IβC and -IαC each bound MPP  $\approx 1.5$ -fold less tightly than

GMPP or GMPP<sub>2</sub> (SI Fig. 5), indicating only a minor contribution from the NAG moiety present in both GMPP and GMPP<sub>2</sub>, but not in MPP. Neither PGRP-IβC nor -IαC bound MPP-Dap, even under conditions at which interactions with *K*<sub>b</sub> > 100 M<sup>-1</sup> should be detectable (19, 20). Thus, both these PGRP domains appear highly specific for Lys-type PGN. By contrast, PGRP-S preferentially recognized MPP-Dap over MPP. In addition, the NAG moiety of GMPP improved affinity  $\approx 14$ -fold relative to MPP, showing that the extra saccharide contributes substantially more to PGN binding in the case of PGRP-S than of PGRP-IβC or -IαC (Table 1). Notably, all three PGRPs bound GMPP<sub>2</sub>, the ligand most representative of natural PGN, with comparable *K*<sub>b</sub>s.

**Overview of the Structure.** The structures of PGRP-IβC in free form and bound to GMPP were determined to resolutions of 2.2 and 2.1 Å, respectively (SI Table 3). The asymmetric unit of the PGRP-IβC-GMPP crystal contains three PGRP-IβC molecules; however, only one forms a complex with GMPP because the binding sites of the other two are blocked by neighboring PGRP-IβC molecules. Obvious electron density corresponding to the entire GMPP ligand was found in the binding cleft, as evident from  $2F_o - F_c$  and  $F_o - F_c$  electron density maps (Fig. 2A). After refinement, the site occupancy was set to 1.0 and the average temperature factor (*B*) was 38.4 Å<sup>2</sup>, compared with 29.6 Å<sup>2</sup> for main-chain atoms (SI Table 3). Superposition of unbound PGRP-IβC domains from both structures onto PGRP-IβC-GMPP gave rms differences in α-carbon positions of 0.23–0.48 Å, indicating no substantial conformational changes upon binding. PGRP-IβC shows a typical PGN-binding domain scaffold (6), in which six β-strands (β3–7) compose a central β-sheet surrounded by three α-helices (α1–3) and two short 3<sub>10</sub> helices (η1 and η2) (Fig. 2A). Three disulfide bonds cross-link the protein.

**Characteristics of the PGN-Binding Cleft.** The PGN-binding site of PGRP-IβC, whose general topology is maintained in other PGRPs (15, 21–28), resides in a long cleft whose walls are formed by helix α1 and five loops (β3–α1, 1α–β4, β5–β6, β6–α2, β7–α3) that project above the central β-sheet platform (Fig. 2A and B). The groove is  $\approx 27$  Å long, with a shallow ( $\approx 6$  Å) end flanked by helix α1 and loops β3–α1 and β6–α2 and a deep ( $\approx 12$  Å) end flanked by loops 1α–β4, β5–β6, and β7–α3. There are two main structural differences between the PGN-binding sites of PGRP-IβC and -IαC, which differ in 22 of 41 residues lining the grooves (SI Fig. 6A). First, loops β5–β6 and β7–α3, which form one wall, provide a broader surface for accommodating NAG in the PGRP-IβC-GMPP complex. Second, the C-terminal portion of helix α1 is displaced away from the PGN-binding site in PGRP-IβC compared

**Table 1.** Binding constants ( $\times 10^3 \text{ M}^{-1}$ ) of PGN derivatives to human PGRPs at 275–277 K

Protein	GMPP	GMPP <sub>2</sub>	MPP	MPP-Dap
PGRP-IβC	227 (±14)	235 (±10)	118 (±4)	NB
PGRP-IαC	59 (±2)	61 (±2)	45 (±1)*	NB*
PGRP-S	82 (±3)	131 (±7)	6 (±0)*	47 (±6)*

For all PGN derivatives, *n* values ranged from 0.98 to 1.07. Values in parentheses represent uncertainties of fit. NB, no binding detectable.

\*Binding data are from ref. 20.



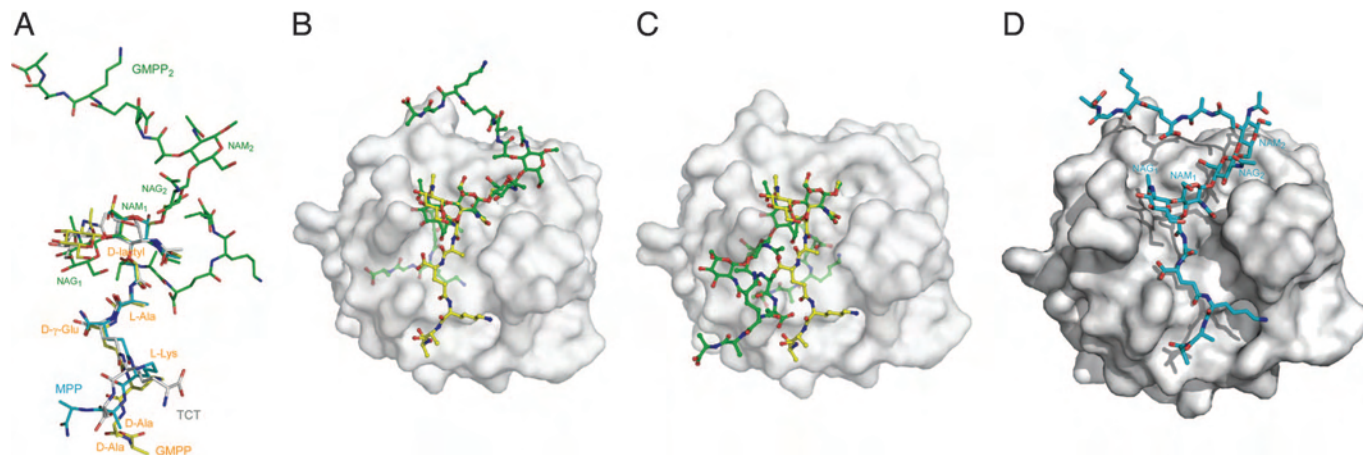


**Fig. 3.** Structural comparison between PGRP-bound PGN analogs in crystal structures and unbound GMPP<sub>2</sub> in solution. (A) Conformational comparison of GMPP, MPP, TCT, and GMPP<sub>2</sub>. GMPP, MPP, and TCT are from crystal structures of complexes with human PGRP-I $\beta$ C, human PGRP-I $\alpha$ C (16), and *Drosophila* PGRP-LE (27), respectively; GMPP<sub>2</sub> is from the unliganded NMR structure (17). The structures are superposed through the pyranose ring of NAM (for MPP, GMPP, and GMPP<sub>2</sub>) or NAM(1,6-anhydro) (for TCT). (B) Superposition of unbound GMPP<sub>2</sub> onto GMPP in the PGRP-I $\beta$ C-GMPP complex. GMPP and GMPP<sub>2</sub> are shown in ball-and-stick representations, with carbon atoms in yellow and green, respectively, nitrogen atoms in blue, and oxygen atoms in red. Of the two GMPP units in GMPP<sub>2</sub>, the first unit, comprising the NAG<sub>1</sub>-NAM<sub>1</sub> disaccharide, is superposed onto GMPP in the complex. The peptide stem of GMPP<sub>2</sub> attached to NAM<sub>1</sub> is buried within PGRP-I $\beta$ C and is shown in pale green. (C) Alternative superposition of unliganded GMPP<sub>2</sub> onto GMPP bound to PGRP-I $\beta$ C. In this case, the second GMPP unit of GMPP<sub>2</sub>, containing NAG<sub>2</sub>-NAM<sub>2</sub>, is superposed onto GMPP in the PGRP-I $\beta$ C-GMPP structure. The peptide stem of GMPP<sub>2</sub> attached to NAM<sub>2</sub>, shown in pale green, is buried inside PGRP-I $\beta$ C. (D) Modeled PGRP-I $\beta$ C-GMPP<sub>2</sub> structure.

maps of the disaccharide 3-Me-4- $\beta$ -NAG- $\alpha$ -NAM (29). Therefore, it appears that the glycan is distorted upon complex formation with PGRP-I $\beta$ C (and other PGRPs). As discussed above, there exist at least two stable minima for the conformation of the D-lactyl moiety. In the PGRP-I $\beta$ C-GMPP structure, the conformation of the D-lactyl moiety of GMPP is similar to that of the PGN monomer (29), with dihedral angles of 67° and -157° for N2(NAM<sub>1</sub>)-C2(NAM<sub>1</sub>)-C3(NAM<sub>1</sub>)-O3(NAM<sub>1</sub>) and C4(NAM<sub>1</sub>)-C3(NAM<sub>1</sub>)-O3(NAM<sub>1</sub>)-C9(D-lactyl), respectively, which differ markedly from those of GMPP<sub>2</sub> (61° and -91°) (Fig. 3A). Other PGRP-bound PGN derivatives (NAM-L-Ala- $\gamma$ -D-Gln-L-Lys, MPP, TCT) also exhibit this conformation for the D-lactyl moiety (15, 16, 27, 28). Thus, it appears that PGRPs consistently favor one of two possible conformations for this residue.

The reason for this preference is evident from superpositions of unbound GMPP<sub>2</sub> (17) onto GMPP in the PGRP-I $\beta$ C-GMPP complex. In Fig. 3B, GMPP<sub>2</sub> is superposed onto GMPP through the first disaccharide (NAG<sub>1</sub>-NAM<sub>1</sub>) of the PGN dimer. However, the peptide stem of GMPP<sub>2</sub> attached to NAM<sub>1</sub> collides with PGRP-I $\beta$ C, requiring the D-lactyl moiety to adopt the conformation observed in unbound PGN monomer (29). Alternatively, GMPP<sub>2</sub> may be superposed onto GMPP through the second disaccharide (NAG<sub>2</sub>-NAM<sub>2</sub>) (Fig. 3C). In this case, the peptide stem of GMPP<sub>2</sub> attached to NAM<sub>2</sub> clashes with the protein, again necessitating a change in orientation relative to the glycan. Importantly, as dis-

cussed below, the PGRP-bound conformation is inconsistent with PGN cross-linking as proposed in a model of the cell wall that is based on the GMPP<sub>2</sub> structure (17).

**Interactions with Polymeric PGN.** PGRP-I $\beta$ C, -I $\alpha$ C, and -S have comparable affinities for GMPP and GMPP<sub>2</sub> (Table 1), suggesting that saccharides beyond NAG<sub>1</sub>-NAM<sub>1</sub> do not contribute substantially to the interaction of PGRPs with PGN. Because we were unable to crystallize PGRP-I $\beta$ C bound to GMPP<sub>2</sub>, we modeled the complex on the basis of the PGRP-I $\beta$ C-GMPP crystal structure, the GMPP<sub>2</sub> solution structure (17), and ITC measurements demonstrating that PGRP-I $\beta$ C, -I $\alpha$ C, and -S all engage GMPP<sub>2</sub> with 1:1 stoichiometry.

In the modeled PGRP-I $\beta$ C-GMPP<sub>2</sub> structure (Fig. 3D), the *N*-acetylamido, hydroxyl, and hydroxymethyl groups of NAG<sub>2</sub>, along with NAM<sub>1</sub> and NAM<sub>2</sub>, restrict the  $\beta$  (1-4) glycosidic dihedral angles between NAM<sub>1</sub> and NAG<sub>2</sub>. The resulting angles of C2(NAM<sub>1</sub>)-C1(NAM<sub>1</sub>)-O1(NAM<sub>1</sub>)-C4(NAG<sub>2</sub>) = 172° and C1(NAM<sub>1</sub>)-O1(NAM<sub>1</sub>)-C4(NAG<sub>2</sub>)-C3(NAG<sub>2</sub>) = 113° are close to those from the NMR structure (173° and 126°, respectively). The  $\beta$  (1-4) glycosidic dihedral angles between NAG<sub>2</sub> and NAM<sub>2</sub> are also well restricted by the *N*-acetylamido, methoxyl, and hydroxymethyl groups of NAM<sub>2</sub>, along with the pentapeptide stem, resulting in angles of 172° and 123°. Under this conformation of NAG<sub>2</sub> and NAM<sub>2</sub>, only NAG<sub>2</sub> can interact with PGRP-I $\beta$ C. In the modeled complex (Fig. 3D), the dihedral angles defining the conformation of the D-lactyl moiety attached to NAM<sub>2</sub> are 59° and -89° for N2(NAM<sub>2</sub>)-C2(NAM<sub>2</sub>)-C3(NAM<sub>2</sub>)-O3(NAM<sub>2</sub>) and C4(NAM<sub>2</sub>)-C3(NAM<sub>2</sub>)-O3(NAM<sub>2</sub>)-C9(D-lactyl), respectively, very similar to those of GMPP<sub>2</sub> in solution (61° and -91°) (17). These angles must differ from those defining the relative orientation of D-lactyl and NAM<sub>1</sub> in GMPP<sub>2</sub> bound to PGRP-I $\beta$ C (66° and -159°) to avoid major collisions between PGRP-I $\beta$ C and the peptide stem. In this way, the stem projects away from the protein, with which it makes no contacts (Fig. 3D). Because only NAG<sub>2</sub> of the NAG<sub>2</sub>-NAM<sub>2</sub>-L-Ala- $\gamma$ -D-Gln-L-Lys-D-Ala-D-Ala repeat of GMPP<sub>2</sub> is predicted to interact with PGRP-I $\beta$ C, the modeled complex is consistent with our finding that the affinity of GMPP<sub>2</sub> for PGRP-I $\beta$ C is no greater than that of GMPP (Table 1). The binding of two PGRP molecules to GMPP<sub>2</sub> would be precluded by

**Table 2. Comparison of selected dihedral angles**

Dihedral angles	PGRP-I $\beta$ C-GMPP	GMPP <sub>2</sub>	PGN monomer
NAG-NAM- $\phi$	163	173	174
NAG-NAM- $\psi$	161	126	118
D-Lac- $\psi$	67	61	66
D-Lac- $\phi$	-157	-91	-159

Definitions for dihedral angles are as follows: NAG-NAM- $\phi$ , C2(NAG<sub>1</sub>)-C1(NAG<sub>1</sub>)-O1(NAG<sub>1</sub>)-C4(NAM<sub>1</sub>); NAG-NAM- $\psi$ , C1(NAG<sub>1</sub>)-O1(NAG<sub>1</sub>)-C4(NAM<sub>1</sub>)-C3(NAM<sub>1</sub>); D-Lac- $\psi$ , N2(NAM<sub>2</sub>)-C2(NAM<sub>2</sub>)-C3(NAM<sub>2</sub>)-O3(NAM<sub>2</sub>); and D-Lac- $\phi$ , C4(NAM<sub>2</sub>)-C3(NAM<sub>2</sub>)-O3(NAM<sub>2</sub>)-C9(D-lactyl). GMPP<sub>2</sub> data are for the NMR structure of GMPP<sub>2</sub> (17). PGN monomer data are for the NMR structure of Dap-type PGN monomer (NAG-NAM-L-Ala- $\gamma$ -D-Gln-Dap-D-Ala-D-Ala) (29).

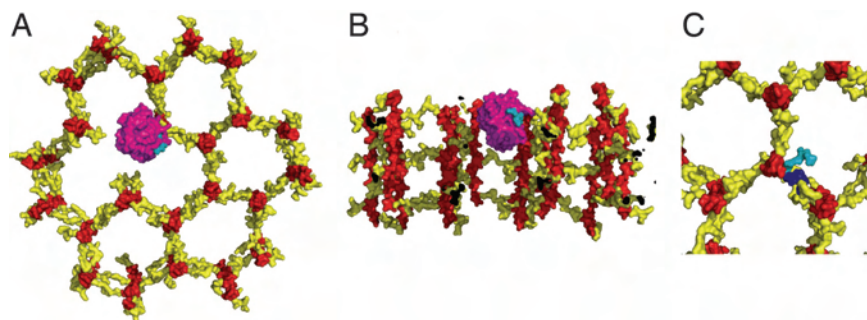


**Fig. 4.** Possible interaction of PGRPs with the bacterial cell wall. (A) Top view of a structural model of a PGRP-I $\beta$ C molecule bound to cell wall PGN. PGRP-I $\beta$ C and the cell wall are shown in molecular surface representation with the glycan strands of PGN in red, the peptide stems in yellow, PGRP-I $\beta$ C in purple, and the PGRP-bound peptide stem in cyan. This model was constructed by docking PGRP-I $\beta$ C onto a GMPP<sub>2</sub> unit of a perpendicular model of the cell wall (17) in which the PGN strands are orthogonal to the cell membrane. The strands form a honeycomb pattern, with pore sizes determined by the extent of cross-linking. Small pores are formed by cross-linking each PGN strand to three neighboring strands. The PGRP-I $\beta$ C molecule is situated in an incompletely cross-linked region of the growing cell wall where a missing PGN strand creates a larger pore. (B) Side view of the model in A, in which the cell wall has been cut away to expose the bound PGRP protein. (C) Comparison of cross-linked and PGRP-bound peptide stems. A cross-linked peptide stem in the model of cell wall PGN is shown in blue. The same peptide stem, but in its PGRP-bound conformation, is shown in cyan.

steric clashes between the proteins, as well as by the imposition of two distinct conformations on the peptide stems of GMPP<sub>2</sub> upon engagement of a single PGRP, only one of which would allow entry of the stem into the PGN-binding groove (Fig. 3B). By contrast, GMPP<sub>2</sub> engages two vancomycins, which are considerably smaller than PGRPs and which interact only with the peptide stems of PGN (18), rather than with both glycan and peptide components, as do PGRPs.

**Mechanistic Implications.** The bacterial cell wall, far from being a static structure, is dynamically turned over during growth (3, 4). In *Escherichia coli*, for example,  $\approx 40\%$  of cell wall components are degraded and recycled per generation (30). Furthermore, the degree of PGN cross-linking varies widely for different bacteria (5–75%) (3, 4). As a consequence, there exists an abundance of free peptide stems available as binding sites for bactericidal agents such as PGRPs.

Our results with the PGRP-I $\beta$ C-GMPP<sub>2</sub> complex may be interpreted in terms of a recent model of cell wall PGN generated *in silico* by using the GMPP<sub>2</sub> solution structure (17). In this model, the glycan strands of PGN are oriented perpendicular to the bacterial cell surface, in sharp contrast to an alternative model that proposes a parallel arrangement (31). A key feature of the perpendicular model is that the PGN strands, whose average length is nine NAG-NAM repeats in *E. coli* (32), form right-handed helices having three NAG-NAM repeats per turn, such that each strand is positioned for cross-linking up to three neighboring PGN strands (17). The result is a honeycomb pattern with pore sizes determined by the extent of cross-linking (Fig. 4A and B). The smallest pores, containing three cross-links, are  $\approx 70$  Å in diameter, whereas missing strands create pores measuring  $\approx 120$  Å (for a single missing strand) or greater (for multiple missing strands). Importantly, all pores with missing strands are sufficiently large to permit a PGN-binding domain, which measures  $\approx 40$  Å, to access and bind to the growing cell wall, despite its relatively large size (Fig. 4A). It is also likely that 120-Å pores, formed by a single missing strand, can accommodate two tandem PGN-binding domains (as found in full-length PGRP-I $\beta$ ), while pores created by two or more missing strands would certainly be able to do so (data not shown). In addition, a growing cell wall should be fully accessible to any PGRP at its outermost edges.

These observations, combined with the demonstration that human PGRPs kill Gram-positive bacteria by directly interacting with their cell wall PGN (10), suggest a mechanism for the bactericidal activity of PGRPs reminiscent of that of vancomycin and related glycopeptide antibiotics. In this view, PGRPs disrupt cell wall

formation by binding the NAG-NAM-L-Ala- $\gamma$ -D-Glu-L-Lys-D-Ala-D-Ala repeat of Lys-type PGN, thereby sterically encumbering access of biosynthetic enzymes to the nascent PGN chains. The net result is inhibition of transglycosylase-catalyzed glycan lengthening and/or transpeptidase-catalyzed cross-linking of peptide stems, leaving the cell susceptible to osmotic lysis. Indeed, PGRP-mediated killing of *Staphylococcus aureus* is prevented in medium containing 0.75 M sucrose (10). Although we have interpreted our results in terms of the perpendicular model of cell wall PGN (17), similar considerations should apply to the parallel model (30).

Beyond simple steric encumbrance, however, the PGRP-I $\beta$ C-GMPP<sub>2</sub> structure further suggests that human PGRPs might disrupt PGN synthesis by locking PGN into a conformation that could prevent formation of cross-links between peptide stems in the growing cell wall. Because newly elongated glycan strands are not cross-linked, this portion of the cell wall will be mechanically fragile until transpeptidation has occurred (13, 14). Free PGN (as represented by GMPP<sub>2</sub>) differs from PGRP-bound PGN with respect to the conformation of the D-lactyl group, which substantially alters the relative orientation of saccharide and peptide moieties (Fig. 3A). In terms of our model of PGRP-I $\beta$ C bound to the cell wall, the effect of this alteration is to position the PGRP-bound peptide such that it is no longer directed toward the peptide of a neighboring PGN strand, with which it could otherwise potentially form a cross-link (Fig. 4C).

Thus, the PGRP-bound conformation of the D-lactyl moiety of PGN appears incompatible with peptide cross-linking, as envisaged in the perpendicular model of the cell wall built using the GMPP<sub>2</sub> structure (17). However, as discussed above, PGN fragments in solution can also adopt a second conformation for the D-lactyl moiety that is of comparable stability to the first (29). It is this second conformation that is exclusively observed in PGRP-PGN complexes (Fig. 3A), implying that PGRPs have evolved to disrupt cell wall formation not only by direct steric inhibition of biosynthetic enzymes, but by favoring an orientation of the peptide stems that reduces their availability for the cross-linking reaction.

## Methods

**PGN Derivatives.** Procedures for synthesizing PGN analogs NAG-NAM-L-Ala- $\gamma$ -D-Glu-L-Lys-D-Ala-D-Ala, NAG-NAM(-L-Ala- $\gamma$ -D-Glu-L-Lys-D-Ala-D-Ala)-NAG-NAM(-L-Ala- $\gamma$ -D-Glu-L-Lys-D-Ala-D-Ala), NAM-L-Ala- $\gamma$ -D-Gln-L-Lys-D-Ala-D-Ala, and NAM-L-Ala- $\gamma$ -D-Gln-Dap-D-Ala-D-Ala have been described in refs. 33–35.

**PGRP Production.** Human PGRP-S and -I $\alpha$ C were obtained by *in vitro* folding from *E. coli* inclusion bodies as described in refs. 21 and 22. A DNA fragment encoding residues 209–373 of PGRP- $\beta$  was cloned into pT7–7 (Novagen, San Diego, CA). The protein was expressed as inclusion bodies in *E. coli* BL21(DE3) cells (Invitrogen, Carlsbad, CA). Inclusion bodies were dissolved in 50 mM Tris-HCl (pH 8.0), 8 M urea, 2 mM EDTA, and 5 mM DTT. Solubilized PGRP-I $\beta$ C was diluted into 1.0 M arginine, 100 mM Tris-HCl (pH 8.5), 2 mM EDTA, 6.3 mM cysteamine, and 3.7 mM cystamine to 50  $\mu$ g/ml. After 3 days at 4°C, the folding mixture was dialyzed against 50 mM Tris-HCl (pH 8.5), and the protein was purified using MonoQ and Superdex 75 HR columns (Amersham Biosciences, Piscataway, NJ).

**ITC Measurements and Analysis.** Thermodynamic parameters for the binding of PGRPs to PGN derivatives were determined using a MicroCal VP-ITC titration calorimeter as described in ref. 20. For the present titrations, *c* values (the product of the initial PGRP concentration and  $K_b$ ) ranged from 3.06 to 7.99, allowing for precise determination of  $K_b$  (19, 36).

**Crystallization and Data Collection.** Crystals of free PGRP-I $\beta$ C (10 mg/ml) grew at room temperature in 0.1 M NiSO<sub>4</sub> and 15% (wt/vol) PEG-3350. Crystals of the PGRP-I $\beta$ C-GMPP complex grew in 15% (vol/vol) Tacsimate (Hampton Research, Riverside, CA), 0.1 M Hepes (pH 7.0), and 2% (wt/vol) PEG-3350 from solutions containing a 3-fold molar excess of GMPP. Both crystals were cryoprotected by soaking in reservoir solutions containing 10% (wt/vol) sucrose. Diffraction data were collected in-house at 100 K by using an R-Axis IV<sup>++</sup> image plate detector (Rigaku, Tokyo, Japan). The data were processed using d\*TREK incorporated in the CrystalClear version 1.35 software suite (Molecular Structure, The Woodlands, TX) (SI Table 3).

**Structure Determination and Refinement.** The structure of unliganded PGRP-I $\beta$ C was solved by molecular replacement with the program Molrep (37). A homology modeled structure of PGRP-I $\beta$ C (38), on the basis of the structure of PGRP-I $\alpha$ C (21) [Protein Data Bank (PDB) ID code 1SK3], was used as the search probe.

Two obvious solutions corresponding to two PGRP-I $\beta$ C monomers in the asymmetric unit resulted in a correlation coefficient of 0.53 and  $R_{\text{cryst}}$  of 48.5% at 30.0–3.0 Å. Refinement was performed using CNS (39). After initial rigid-body refinement, the correlation coefficient was 0.67, and  $R_{\text{cryst}}$  was 45.3%. Manual model rebuilding was carried out in XtalView (40) on the basis of  $\sigma_A$ -weighted  $2F_o - F_c$  and  $F_o - F_c$  electron density maps. The final model has  $R_{\text{cryst}}$  of 22.9% and  $R_{\text{free}}$  of 28.5% at 2.2-Å resolution (SI Table 3).

The structure of the PGRP-I $\beta$ C-GMPP complex was determined by molecular replacement using the structure of unliganded PGRP-I $\beta$ C as the probe. Three PGRP-I $\beta$ C molecules were unambiguously located in the asymmetric unit with a correlation coefficient of 0.67 and  $R_{\text{cryst}}$  of 51.3% at 30.0–3.0 Å. Refinement was carried out as above, but only one GMPP molecule could be identified from  $\sigma_A$ -weighted  $2F_o - F_c$  and  $F_o - F_c$  electron density maps. The single GMPP was fitted into the density and refinement performed. The final  $R_{\text{cryst}}$  is 21.0% and  $R_{\text{free}}$  is 24.2% at 2.1-Å resolution (SI Table 3).

**Modeling of Human PGRP-I $\beta$ C-GMPP<sub>2</sub> Complex.** Two saccharides (NAG<sub>2</sub> and NAM<sub>2</sub>) were added one by one to the PGRP-I $\beta$ C-GMPP crystal structure, maintaining the  $\beta$ (1–4) glycosidic dihedral angles of C2(NAG<sub>1</sub>)–C1(NAG<sub>1</sub>)–O1(NAG<sub>1</sub>)–C4(NAM<sub>1</sub>) = 173° and C1(NAG<sub>1</sub>)–O1(NAG<sub>1</sub>)–C4(NAM<sub>1</sub>)–C3(NAM<sub>1</sub>) = 126°, which correspond to the NMR structure of GMPP<sub>2</sub> (17). Each saccharide addition was followed by 200 cycles of steepest descent minimization and 300 cycles of conjugate gradient minimization in AMBER 7 (41). GMPP<sub>2</sub> was allowed to move freely, the side chains of residues immediately surrounding GMPP<sub>2</sub> were permitted to move, and the rest of PGRP-I $\beta$ C was fixed. After two saccharides were added, the pentapeptide stem was attached to NAM<sub>2</sub> with dihedral angles of 61° and –91° for N2(NAM<sub>2</sub>)–C2(NAM<sub>2</sub>)–C3(NAM<sub>2</sub>)–O3(NAM<sub>2</sub>) and C4(NAM<sub>2</sub>)–C3(NAM<sub>2</sub>)–O3(NAM<sub>2</sub>)–C9(D-lactyl) (17), and the entire structure was subjected to energy minimization.

This work was supported by National Institutes of Health Grants GM065248 (to G.-J.B.), AI047990, AI065612 (both to R.A.M.), and GM61629 (to S.M.).

1. Medzhitov R, Janeway CA, Jr (2002) *Science* 296:298–300.
2. Hoffmann JA (2003) *Nature* 426:33–38.
3. Schleifer KH, Kandler O (1972) *Bacteriol Rev* 36:407–477.
4. Doyle RJ, Dziarski R (2001) in *Molecular Medical Microbiology*, ed Sussman M (Academic, London), pp 137–153.
5. Royet J, Dziarski R (2007) *Nat Rev Microbiol* 5:264–277.
6. Guan R, Mariuzza RA (2007) *Trends Microbiol* 15:127–134.
7. Dziarski R, Platt KA, Gellius E, Steiner H, Gupta D (2003) *Blood* 102:689–697.
8. Cho JH, Fraser IP, Fukase K, Kusumoto S, Fujimoto Y, Stahl GL, Ezekowitz RA (2005) *Blood* 106:2551–2558.
9. Tydell CC, Yuan J, Tran P, Selsted ME (2006) *J Immunol* 176:1154–1162.
10. Lu X, Wang M, Qi J, Wang H, Li X, Gupta D, Dziarski R (2006) *J Biol Chem* 281:5895–5907.
11. Lehrer RI (2004) *Nat Rev Microbiol* 2:727–738.
12. Brogden KA (2005) *Nat Rev Microbiol* 3:238–250.
13. Williams DH, Bardsley B (1999) *Angew Chem Int Ed* 38:1172–1193.
14. Kahne D, Leimkuhler C, Wei L, Walsh C (2005) *Chem Rev* 105:425–448.
15. Guan R, Roychowdhury A, Ember B, Kumar S, Boons G-J, Mariuzza RA (2004) *Proc Natl Acad Sci USA* 101:17168–17173.
16. Guan R, Brown PH, Swaminathan CP, Roychowdhury A, Boons G-J, Mariuzza RA (2006) *Protein Sci* 15:1199–1206.
17. Meroueh SO, Benzec KZ, Heseck D, Lee M, Fisher JF, Stemmler TL, Mobashery S (2006) *Proc Natl Acad Sci USA* 103:4404–4409.
18. Rekharsky M, Heseck D, Lee M, Meroueh S, Inoue Y, Mobashery S (2006) *J Am Chem Soc* 128:7736–7737.
19. Turnbull WB, Daranas AH (2003) *J Am Chem Soc* 125:14859–14866.
20. Swaminathan CP, Brown PH, Roychowdhury A, Wang Q, Guan R, Silverman N, Goldman WE, Boons G-J, Mariuzza RA (2006) *Proc Natl Acad Sci USA* 103:684–689.
21. Guan R, Malchiodi EL, Wang Q, Schuck P, Mariuzza RA (2004) *J Biol Chem* 279:31873–31882.
22. Guan R, Wang Q, Sundberg EJ, Mariuzza RA (2005) *J Mol Biol* 347:683–691.
23. Kim MS, Byun M, Oh BH (2003) *Nat Immunol* 4:787–793.
24. Chang CI, Pili-Floury S, Herve M, Parquet C, Chelliah Y, Lemaitre B, Mengin-Lecreux D, Deisenhofer J (2004) *PLoS Biol* 2:1293–1302.
25. Reiser JB, Teyton L, Wilson IA (2004) *J Mol Biol* 340:907–917.
26. Chang CI, Ihara K, Chelliah Y, Mengin-Lecreux D, Wakasaki S, Deisenhofer J (2005) *Proc Natl Acad Sci USA* 102:10279–10284.
27. Lim J-H, Kim M-S, Kim H-E, Yano T, Oshima Y, Aggarwal K, Goldman WE, Silverman N, Kurata S, Oh B-H (2006) *J Biol Chem* 281:8286–8295.
28. Chang CI, Chelliah Y, Borek D, Mengin-Lecreux D, Deisenhofer J (2006) *Science* 311:1761–1764.
29. Matter H, Szilagy L, Forgo P, Marinic Z, Klacik B (1997) *J Am Chem Soc* 119:2212–2223.
30. Vollmer W, Holtje JV (2004) *J Bacteriol* 186:5978–5987.
31. Goodell EW (1985) *J Bacteriol* 163:305–310.
32. Harz H, Burgdorf K, Holtje JV (1990) *Anal Biochem* 190:120–128.
33. Heseck D, Savorov M, Morio KI, Lee M, Brown S, Vakulenko S, Mobashery S (2004) *J Org Chem* 69:778–784.
34. Heseck D, Lee MJ, Morio KI, Mobashery S (2004) *J Org Chem* 69:2137–2146.
35. Roychowdhury A, Boons G-J (2005) *Tetrahedron Lett* 46:1675–1678.
36. Wiseman T, Williston S, Brandts JF, Lin LN (1989) *Anal Biochem* 179:131–137.
37. Collaborative Computational Project, Number 4 (1994) *Acta Crystallogr D* 50:760–763.
38. Peitsch MC (1996) *Biochem Soc Trans* 24:274–279.
39. Brünger AT, Adams PD, Clore GM, DeLano WL, Gros P, Grosse-Kunstleve RW, Jiang JS, Kuszewski J, Nilges M, Pannu NS, et al. (1998) *Acta Crystallogr D* 54:905–921.
40. McRee DE (1999) *J Struct Biol* 125:156–165.
41. Case DA, Pearlman DA, Caldwell JW, Cheatham TE, III, Wang J, Ross WS, Simmerling CL, Darden TA, Merz KM, Stanton RV, et al. (2002) AMBER 7 (Univ of California, San Francisco).